Statistics of ultrasonic scatterer size estimation with a reference phantom[a)]

Anthony Gerig,[b)] James Zagzebski, and Tomy Varghese
Department of Medical Physics, University of Wisconsin—Madison, 1300 University Avenue, Room 1530, Madison, Wisconsin 53706

(Received 12 September 2002; revised 23 February 2003; accepted 24 February 2003)

A theoretical expression for the variance of scatterer size estimates is derived for a modified least squares size estimator used in conjunction with a reference phantom method for backscatter coefficient measurement. A Gaussian spatial autocorrelation function is assumed. Simulations and phantom experiments were performed to verify the results for backscatter and size variances. The dependence of size estimate errors upon free experimental parameters is explored. Implications of the findings for the optimization of scatterer size estimation are discussed. The utility of scatterer size parametric imaging is examined through the signal to noise ratio comparison with standard ultrasonic B-mode imaging. © *2003 Acoustical Society of America.* [DOI: 10.1121/1.1568945]

PACS numbers: 43.80.Vj, 43.80.Qf [FD]

I. INTRODUCTION

The feasibility of estimating and imaging scatterer size using backscattered ultrasound signals and spectral analysis techniques has been thoroughly demonstrated over the past two decades.[1–6,16] Much of the early work in the field involved the use of single element transducers, although in subsequent years the work progressed to accommodate clinical transducers and systems through the development of novel techniques to account for echo signal system dependencies.[4,7,8] In many cases, size estimation, although computationally intensive, has proven to be useful for the monitoring, diagnosis, and study of disease.[3,4]

The following paper has two objectives. The first is to define the theoretical error associated with ultrasonic scatterer size estimation, and its dependence upon parameters that characterize both the measurement system and the insonified tissue. The results make the optimization of estimate error possible through the informed adjustment of free parameters. Others have investigated size estimation error in previous work.[9,10] Chaturvedi and Insana, in particular, have derived an expression for the variance of scatterer size estimates. However, the results assumed knowledge of both the instrumentation transfer function and the scattering strength of the insonified object. The following work extends their inquiry to a particularly simple and flexible method of scatterer size estimation.[4] A reference phantom is used to account for clinical system dependencies in backscatter estimation, and a modified least squares fit, which eliminates the need for knowledge of scattering strength, is used in size estimation. The second objective is to evaluate scatterer size imaging as a diagnostic tool through signal-to-noise ratio (SNR) comparison with standard B-mode imaging.

The following background section gives a brief introduction to scatterer size estimation using a reference phantom. The subsequent theory and verification sections derive and validate expressions for the error inherent in both backscatter coefficient measurement and size estimation. Finally, the discussion and conclusion sections explore the dependence of errors in size estimates upon experimental parameters, discuss the adjustment of free parameters to achieve error optimization, and outline implications for the diagnostic utility of scatterer size imaging.

II. BACKGROUND—SIZE ESTIMATION METHOD

Size estimation, for the purposes of this paper, is accomplished by performing a modified least squares fit between a measured backscatter coefficient for a tissue segment, and a theoretical backscatter coefficient, which is dependent upon tissue/scatterer properties including size. The scatterer size estimate, $\hat{a}$, is given by

$$\hat{a} = \arg\min \frac{1}{n} \sum_{\omega_{\min}}^{\omega_{\max}} [\psi(\omega,\hat{a}) - \overline{\psi}(\hat{a})]^2 \tag{1a}$$

where

$$\psi(\omega,\hat{a}) = 10\ln[\mathrm{BSC}_s(\omega)] - 10\ln[\mathrm{BSC}_t(\omega)] \tag{1b}$$

and

$$\overline{\psi}(\hat{a}) = \frac{1}{n} \sum_{\omega_{\min}}^{\omega_{\max}} \psi(\omega,\hat{a}). \tag{1c}$$

The summation is over the usable bandwidth of the backscatter coefficient measurement [BSC(ω)], ω represents angular frequency, and the subscripts s and t refer to measured sample and theoretical model values, respectively. Unlike the standard least squares fitting technique, this method is insensitive to differences between measured and theoretical values by a multiplicative constant, and therefore requires no knowledge of tissue scattering strength for accurate size estimation.[6]

A reference phantom method is used for backscatter estimation.[4,8,18] Backscatter coefficients are calculated according to

[a)]Presented as "Statistics of scatterer size estimation," *Symposium on Ultrasonic Imaging and Tissue Characterization*, Arlington, VA, June 2002.

[b)]Author to whom correspondence should be addressed. Electronic mail: algerig@wisc.edu

 0001-4966/2003/113(6)/3430/8/$19.00

$$\hat{\mathrm{BSC}}_s(\omega)=\frac{\overline{|S_s(\omega)|^2}}{\overline{|S_r(\omega)|^2}}\mathrm{BSC}_r(\omega)\exp\{4z[\alpha_s(\omega)-\alpha_r(\omega)]\}, \quad (2)$$

where $|S(\omega)|^2$ is the power spectrum for a gated rf signal from a segment of the scattering medium, z is the depth of that segment, and the α 's are attenuation coefficients. The bars represent spatial averages, and the subscripts s and r represent the sample and reference media, respectively. Reference media can be of any type, given that the backscatter coefficient is known and that scattering is incoherent. This method yields accurate results given that the distance from the transducer to the interrogated medium segment is larger than both the size of the active transducer face, and the effective width of the medium spatial autocorrelation function (SAF).[8] System settings must also remain unchanged between reference and sample data acquisition.

The theoretical backscatter coefficient values required for Eq. (1) can be obtained as a function of scatterer size using

$$\mathrm{BSC}(k)=Ck^4\int_{-\infty}^{\infty}b_\gamma(\Delta\mathbf{r})e^{-i2\mathbf{k}\cdot\Delta\mathbf{r}}d\Delta\mathbf{r}, \quad (3)$$

which is valid for sparse media when scattering is weak, and shear wave effects are negligible.[6,11] C is a function of tissue properties and is constant with frequency. $\mathbf{k}$ is the scattering vector, which has magnitude $k=$ wave number and points in the direction of insonification. $b_\gamma(\Delta\mathbf{r})$ is the correlation coefficient of the medium SAF, which is assumed to be statistically stationary and is defined according to $E\{\gamma(\mathbf{r}+\Delta\mathbf{r}),\gamma(\mathbf{r})\}=E\{\gamma^2(\mathbf{r})\}b_\gamma(\Delta\mathbf{r})$. $\gamma(\mathbf{r})$ is the reflectivity of the medium at $\mathbf{r}$, and is a function of the fluctuation in material acoustic properties at that location, $\gamma(\mathbf{r})=(\kappa(\mathbf{r})-\kappa_0)/\kappa_0-(\rho(\mathbf{r})-\rho_0)/\rho(\mathbf{r})$. κ and ρ are compressibility and density, respectively, and κ_0 and ρ_0 are their corresponding mean values for the medium.

For random media with a single dominant scatterer type, the integral of the correlation coefficient can be properly associated with scatterer volume. As a result, an effective scatterer size can be related to the characteristic dimension of the medium correlation coefficient by equating the volume of a sphere to the coefficient integral.[6,11] Throughout the remainder of this paper, only sample media whose correlation coefficients are adequately described by an isotropic Gaussian function will be addressed.[5,6] Thus,

$$b_\gamma(\Delta r)=e^{-\Delta r^2/2d^2}, \quad (4)$$

where the following describes the relationship between effective scatterer radius and the characteristic dimension of the correlation coefficient, d:

$$2a=(12\sqrt{2\pi})^{1/3}d\approx 3.1d=d_1d. \quad (5)$$

The backscatter coefficient for such a medium is given by

$$\mathrm{BSC}(k)=C'k^4e^{-2k^2d^2}, \quad (6)$$

where the frequency dependence is determined solely by effective scatterer size. It is this property, which, in conjunction with the use of the modified least squares fitting technique outlined in Eq. (1), permits size estimation without knowledge of other descriptive parameters for the insonified medium.

III. THEORY

Before calculating the expected error in size estimates for the procedure outlined above, it is necessary to derive an expression for the variance of BSC estimates obtained using the reference phantom method. Neglecting windowing effects and assuming that both sample and reference spectra are estimated using a periodogram, spectra variances are given by[9]

$$\mathrm{var}(\hat{S}(k))\approx S(k)^2. \quad (7)$$

$S(k)$ is an arbitrary power spectrum, and k is the wave number. Given this result and Eq. (2), the variance of the backscatter estimates can be evaluated using[12]

$$\mathrm{var}(\hat{\mathrm{BSC}}_s(k))\approx\left(\frac{\partial(\hat{\mathrm{BSC}}_s(k))}{\partial(\overline{S_s(k)})}\right)^2\mathrm{var}(\overline{S_s(k)})+\left(\frac{\partial(\hat{\mathrm{BSC}}_s(k))}{\partial(\overline{S_r(k)})}\right)^2\mathrm{var}(\overline{S_r(k)}), \quad (8)$$

where $\overline{S_s(k)}$ and $\overline{S_r(k)}$ are independent. Calculating the partial derivatives at expected values, and assuming that the individual power spectra used to obtain the sample and reference averages are independent, yields

$$\mathrm{var}(\hat{\mathrm{BSC}}_s(k))\approx\left[\frac{1}{S_r(k)}\mathrm{BSC}_r(k)e^{4(\alpha_s-\alpha_r)z}\right]^2\frac{1}{N_s}S_s^2(k)+\left[\frac{S_s(k)}{S_r^2(k)}\mathrm{BSC}_r(k)e^{4(\alpha_s-\alpha_r)z}\right]^2\frac{1}{N_r}S_r^2(k), \quad (9)$$

where N_s and N_r represent the number of sample and reference waveforms used to calculate the spectral averages, respectively. Finally, substituting

$$S(k)=|G(k)|^2\mathrm{BSC}(k)e^{-4\alpha z}, \quad (10)$$

where $|G(k)|^2$ is the system transfer function, gives

$$\mathrm{var}(\hat{\mathrm{BSC}}_s(k))\approx\left(\frac{N_s+N_r}{N_sN_r}\right)\mathrm{BSC}_s^2(k). \quad (11)$$

According to this result, the standard deviation of backscatter estimates should be both proportional to the backscatter coefficient itself, and inversely proportional to the square root of the number of data segments used to generate those estimates. Note that Eq. (11) is nearly identical to the result derived by Chaturvedi *et al.*,[9] but contains the additional leading factor, which accounts for both imperfect knowledge of the reference power spectrum, and the possibility of the availability and utilization of multiple sample power spectra.

Solving Eq. (1) for estimated scatterer size, assuming a Gaussian correlation coefficient and using a standard calculus minimax approach,[17] yields

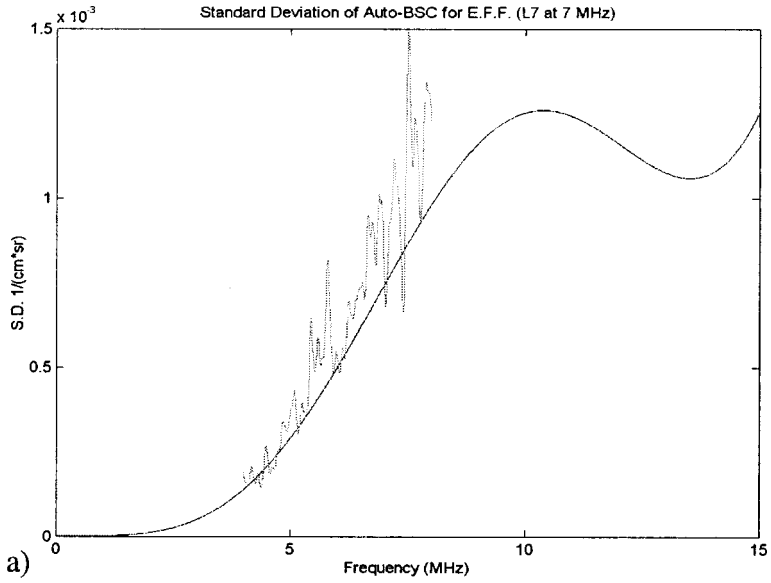

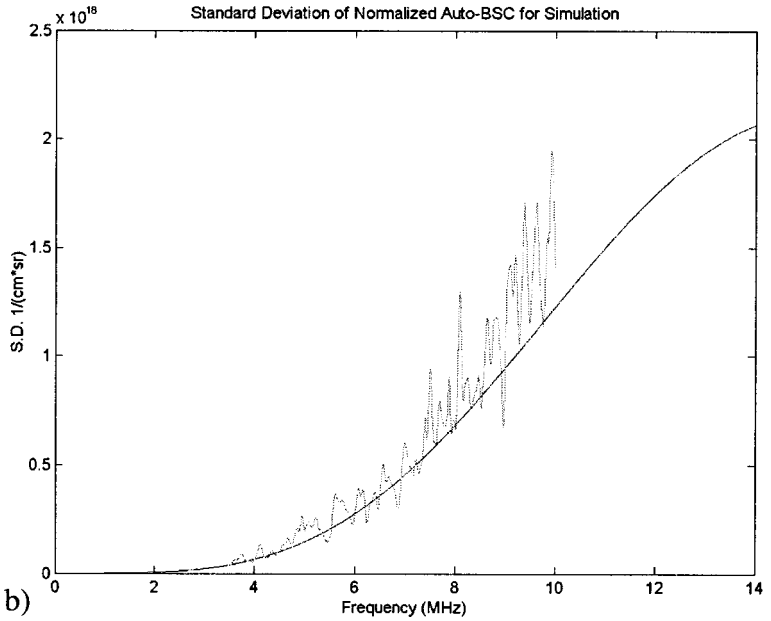

FIG. 1. Theoretical and experimental standard deviations of backscatter coefficient estimates for a tissue-mimicking phantom containing glass beads (a) and a simulated phantom containing scatterers with a Gaussian spatial autocorrelation function (b). The term Auto-BSC indicates that backscatter estimates were generated using reference and sample waveforms from the same phantom.

$$\hat{a}^2 = \frac{-d_1^2 c^2}{80} \frac{\Sigma_{\omega_{\min}}^{\omega_{\max}} (y(\omega)\omega^2 - \overline{y}\,\overline{\omega^2})}{\Sigma_{\omega_{\min}}^{\omega_{\max}} (\omega^2 - \overline{\omega^2})^2}, \tag{12}$$

where $y(\omega) = 10 \ln(\mathrm{BSC}(\omega)/\omega^4)$, c is the speed of sound, and d_1 remains from Eq. (5). For real values of scatterer size, using[12]

$$\mathrm{var}(\hat{a}) \approx \sum_{\omega_{\min}}^{\omega_{\max}} \left(\frac{\partial \hat{a}}{\partial\, \mathrm{BSC}(\omega)} \right)^2_{\mathrm{BSC}(\omega,\hat{a})} \mathrm{var}(\mathrm{BSC}(\omega)), \tag{13}$$

in conjunction with Eqs. (12) and (11) yields

$$\mathrm{var}(\hat{a}) \approx \frac{c^4 d_1^4}{16^2 \hat{a}^2} \left(\frac{N_s + N_r}{N_s N_r} \right) \sum_{\omega_{\min}}^{\omega_{\max}} \left[\frac{\omega^2 - \overline{\omega^2}}{\Sigma_{\omega_{\min}}^{\omega_{\max}} (\omega^2 - \overline{\omega^2})^2} \right]^2, \tag{14}$$

where the summation is limited to frequencies for which the associated backscatter estimates are uncorrelated. When the reference phantom method, in particular, is used to estimate backscatter over a frequency band, the interval between uncorrelated estimates is a function of data window type, and is inversely proportional to window length. Note that this approximation is valid for any particular experimental case, given that the probability for obtaining imaginary size estimates is low, and that size estimates are unbiased.

IV. EXPERIMENTAL VERIFICATION

A. Frequency dependence of backscatter variance

The frequency dependence of Eq. (11) was verified using both simulated rf waveforms, and experimentally derived signals obtained from an agar phantom. The phantom con-

tained spherical glass scatterers of mean diameter 48 μm and standard deviation 6.8 μm, distributed randomly with a density of 1.36 g/L (approximately 10 000 scatterers/cm^3). The speed of sound and attenuation for the phantom, both measured using a narrow-band substitution technique, were 1490 m/s and 0.5 dB/cm/MHz, respectively. The agar density was calculated to be 1.04 g/cm^3. Thirty independent planes of phantom data were acquired using an Acuson 128 XP and L7 linear array transducer operating at 7 MHz. System settings remained unchanged throughout the data collection procedure. The rf echo signals were digitized with a Gage Applied Science (Canada) A/D converter and PC. Data were collected with 12-bit resolution and at a sampling rate of 50 MHz.

Eleven independent planes of simulated rf data were generated for a random distribution of Gaussian SAF scatterers (4000/cm^3) with effective diameters of 50 μm. To accomplish this, the scattered pressure amplitudes at each frequency for simulated pointlike scatterers were modified by multiplication with the square root of the form factor for a Gaussian SAF, $e^{-k^2d^2}$, where d is related to the scatterer size through Eq. (5). The phantom speed of sound was set to 1490 m/s and the attenuation to zero.[15] The simulated transducer was a 300-line linear array operating at 7 MHz with a 50 mm focal length and 100% bandwidth, which could be artificially reduced during processing. The data acquisition rate was 38 MHz (a value determined by the simulation code).

Backscatter estimates for both the agar and simulated phantoms were generated according to the reference phantom method outlined in Sec. II. In both cases, the reference and sample phantoms were identical, eliminating the need for an attenuation correction term in Eq. (2). Power spectral estimates for each waveform were calculated using a 1 cm Hanning windowed segment centered about the transducer transmit focus (3.5 cm for the L7, 5 cm for the simulation). Spectral averaging for each transducer line was done over independent planes. Fifteen reference and sample planes were used for the agar phantom estimates, and one sample and ten reference planes for the simulation estimates. Standard deviation estimates at each frequency were made using the backscatter estimates obtained for each of the transducer lines (220 for the L7, 300 for the simulated transducer).

Results are plotted in Fig. 1. Theoretical values were calculated using Eq. (11), where the known backscatter coefficient originates from Faran's theory[13] for the agar/glass phantom, and the SAF input for the simulation. Agreement between theoretical and experimental values for both cases appears to be good over the bandwidth of the transducer used. The slight bias at higher frequencies is a result of backscatter estimate bias, which, in turn, is due to the inherent noise in the reference spectral estimates. Including additional reference spectral estimates in the spatial averaging of Eq. (2) reduces this effect.

B. Dependence of backscatter variance upon the number of spectral estimates

Log transformation of both the standard deviation for backscatter estimates and the number of spectra used to generate those estimates in Eq. (11), assuming equal numbers of reference and sample waveforms, yields

$$\log\{\mathrm{std}[\hat{\mathrm{BSC}}(k,N)]\} = -\tfrac{1}{2}\log(N) + C(k).$$

According to this equation, the relationship between the two transformed values is a linear one defined by a slope of negative one-half. This was verified experimentally using the same phantom data and signal processing method described above. Standard deviation estimates, however, were generated using variable numbers of sample and reference waveforms ($N_s = N_r = N = 5-15$). The slope of the linear least squares fit to the log of standard deviation estimates versus the log of the number of spectra used in generating those estimates was calculated for each frequency resulting from

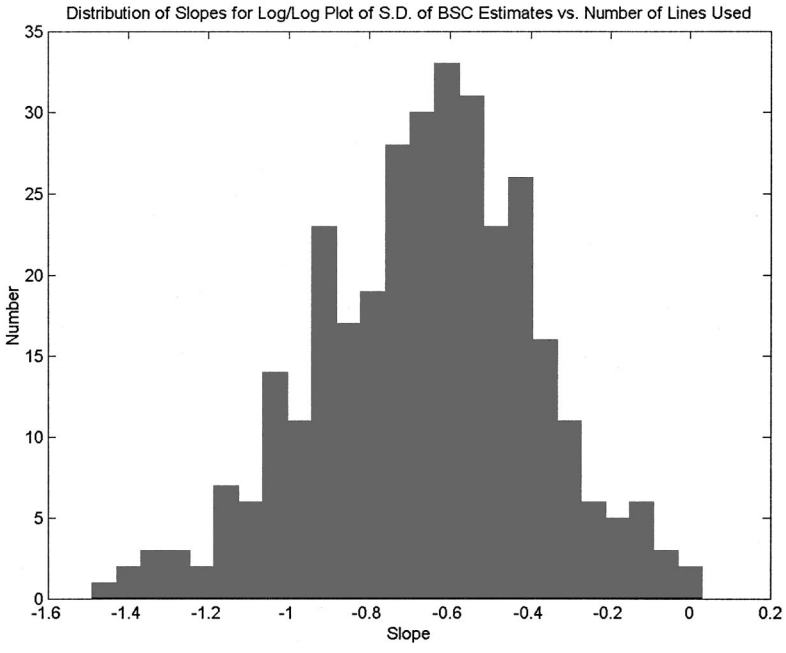

FIG. 2. Histogram of linear regression slopes (each obtained at a different frequency) for the log of the standard deviation of backscatter coefficient estimates as a function of the log of the number of A lines used to generate those estimates.

the discrete Fourier transform of the rf data over the bandwidth of the L7 transducer. A histogram of those slopes is plotted in Fig. 2. Note that the approximate center of the distribution is negative one-half, as theory predicts.

C. Size variance

The validity and accuracy of Eq. (14) were tested using the simulated waveforms described in Sec. IV A, with the inclusion of waveforms from several additional independent planes. Windowed data segments used in backscatter estimation were again centered about the transmit focus of the transducer (5 cm for simulated data). Size estimates were obtained using the method outlined in Eq. (1), with the modified sum of squares value being calculated for a restricted range of possible scatterer sizes (diameter=1–300 μm in intervals of one micron). As a result, imaginary size estimates were excluded. Standard deviation estimates were generated using 300 partially correlated size estimates corresponding to the number of lines produced by the simulated linear transducer. Note that all estimated backscatter values, including correlated ones, were used in size estimation.

Figure 3(a) displays both theoretical and experimental results for the standard deviation of size estimates as a function of the bandwidth used to produce those size estimates. Ten reference and one sample waveform segments (eleven independent planes of data total), each one cm in length, were used to generate the necessary backscatter estimates. The theoretical result was calculated using Eq. (14). The frequency interval for which uncorrelated backscatter estimates could be obtained was determined experimentally by estimating the correlation of those estimates, and found to be approximately 2.4/T for complete decorrelation, where *T* corresponds to the length of the Hanning window used in units of time. The resulting number of uncorrelated frequencies included in the summation of Eq. (14) as a function of bandwidth was noticeably steplike, leading to the discontinuities evident in the theoretical curve. With the exception of the estimate at 3 MHz, the experimental and theoretical results agree well. The most likely explanation for the poor agreement at low bandwidths is that imaginary estimates would typically play a dominant role in this region for scatterers of this size. As a result, the conditions for the validity of Eq. (14) are not met, and the experimental standard deviation is artificially limited by the exclusion of imaginary estimates.

Figure 3(b) shows similar results for a fixed bandwidth of 6 MHz, but a variable number of sample waveforms. Ten reference waveforms were used throughout. Again, theoretical and experimental results agree fairly well.

Finally, Fig. 3(c) contains results for a fixed bandwidth of 6 MHz, a fixed number of waveforms (10 reference and 1 sample), and a variable data window length. The theoretical and experimental results agree well for larger window sizes. For lengths shorter than 4 cm, the results diverge for what is likely the same reason they do so in Fig. 3(a) for shorter bandwidths, namely that imaginary estimates typically become more prevalent as the standard deviation for estimation approaches the scatterer diameter value. Equation (14) therefore ceases to be valid, and the experimental standard deviation is limited.

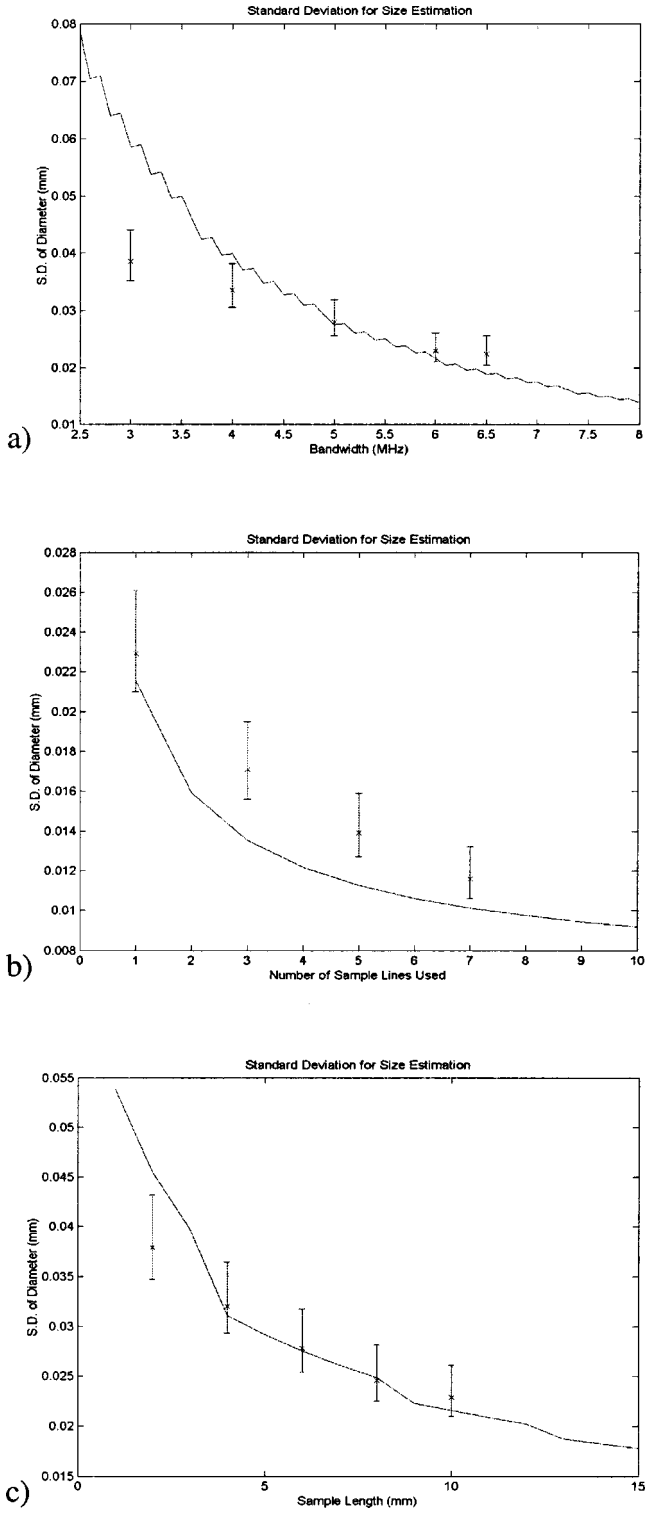

FIG. 3. Theoretical predictions and experimental results for the standard deviation of scatterer size estimates as a function of transducer bandwidth (a), the number of sample A lines used (b), and A-line length (c). Error bars are located approximately at alpha=0.5.

V. DISCUSSION

A. Optimization

Given the demonstrated accuracy and applicability of Eq. (14), it becomes possible to use the equation to optimize

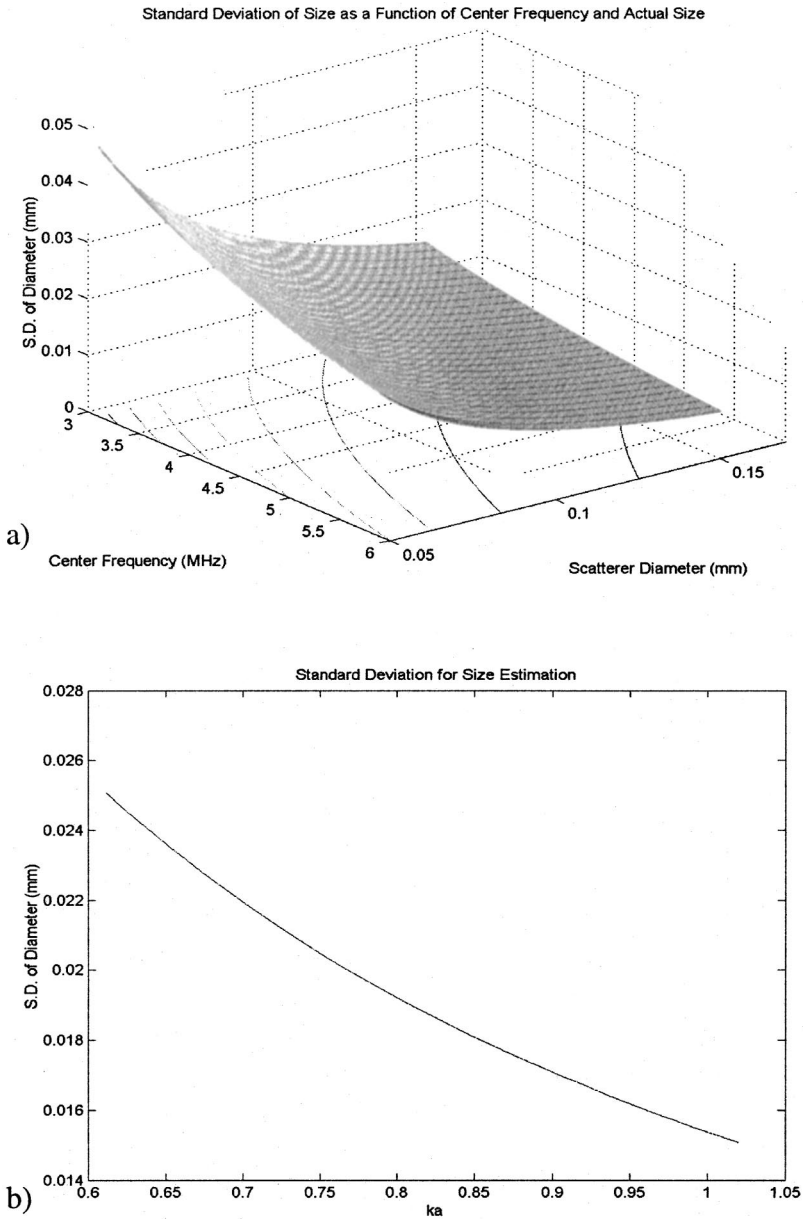

FIG. 4. Mesh and contour plots of the theoretical standard deviation of scatterer size estimates as a function of transducer center frequency and actual scatterer size (a). (b) displays standard deviation as a function of the product of the two parameters.

experimental parameters for the minimization of uncertainty in size estimates. As is obvious from Fig. 3, monotonic decreases in standard deviation are associated with increases in transducer bandwidth, the number of independent sample (and reference) waveforms used to generate backscatter estimates, and window length. Increases in the first of these are limited by the capabilities of the imaging system. Changes in the second are generally restricted both by the inherent resolution of the system, and the desired resolution of the scatterer size image. Finally, the window length is constrained by the desired axial resolution of the resultant image.

Two parameters remain in Eq. (14). The first of these is transducer center frequency, and the second is actual scatterer size. Figure 4(a) displays estimate standard deviation as a function of both parameters for a bandwidth of 6 MHz, a window length of 1 cm, a single sample waveform, and ten reference waveforms. Below the mesh plot of standard deviation is a contour plot of the same, the isobars of which correspond approximately to constant values of the product of the two independent variables. As a result of this correspondence, the dependence of Eq. (14) upon the two separate parameters appears to reduce to a dependence upon one, namely *ka*, where *k* is the wave number corresponding to the center frequency value, and *a* the actual scatterer radius. Figure 4(b) illustrates the dependence of the standard deviation upon *ka* for a 6 MHz bandwidth, a 1 cm window, one sample waveform, and ten reference waveforms. Because the standard deviation is inversely proportional to *ka*, optimization would entail size estimation at high frequencies. However, failure of the Gaussian SAF to appropriately model scatterer behavior at high frequencies places an upper limit upon *ka* of approximately 1.2. At frequencies above this limit, shear wave and resonance effects, which are not included in the scattering model, become appreciable.[2,6,11]

B. Evaluation

To evaluate size estimation, and the method outlined in this paper in particular, as a diagnostic aid, the SNR for a

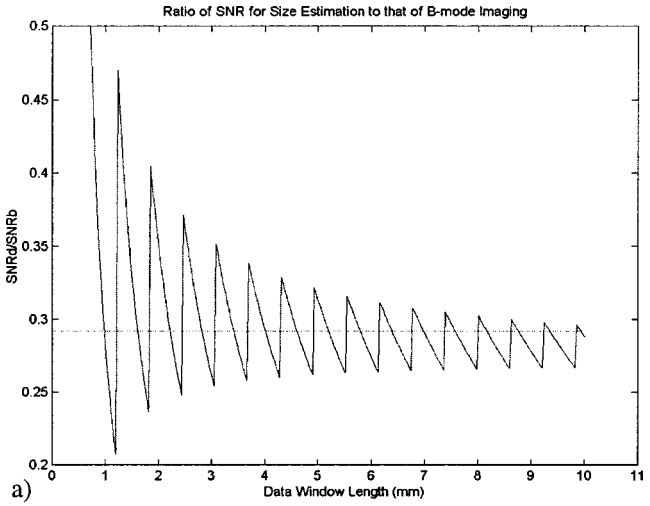

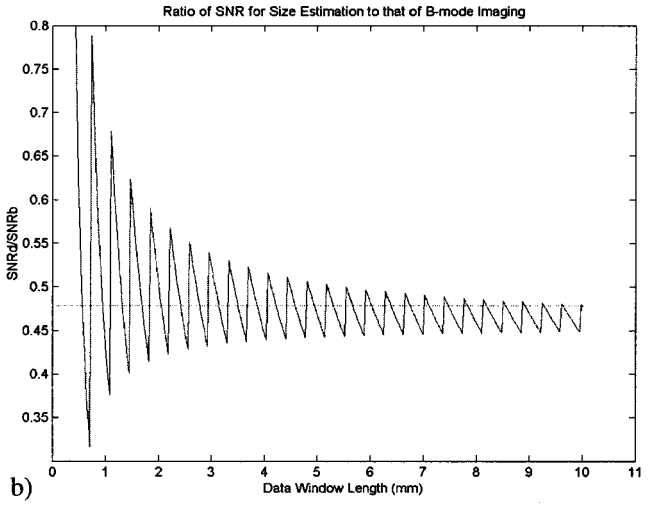

FIG. 5. Ratios of the theoretical signal-to-noise for size estimation to that of B-mode imaging for bandwidths of 3 MHz (a) and 5 MHz (b). A horizontal line is located at the mean value of the ratio over the plotted function domain in each case.

parametric image of size was compared to that for a standard B-mode image of identical resolution. The SNR for the scatterer size image was defined as

$$\mathrm{SNR}_d = \frac{E(\hat{D})}{\mathrm{std}(\hat{D})}, \tag{15}$$

where $E(\hat{D})$ and $\mathrm{std}(\hat{D})$ are the expected value and standard deviation of the size estimator, respectively. The SNR for a B-mode image with fully developed speckle is

$$\mathrm{SNR}_b = 1.91\sqrt{\frac{T}{C_z}}, \tag{16a}$$

where 1.91 is the SNR for a single resolution cell, and the square root factor corrects for differences in axial resolution between the two image types. T is the window length used in size estimation, C_z is the axial length of a resolution cell, and their quotient is the number of uncorrelated cells contained within a single window. C_z is related to the bandwidth of the insonifying transducer and is approximated by[14]

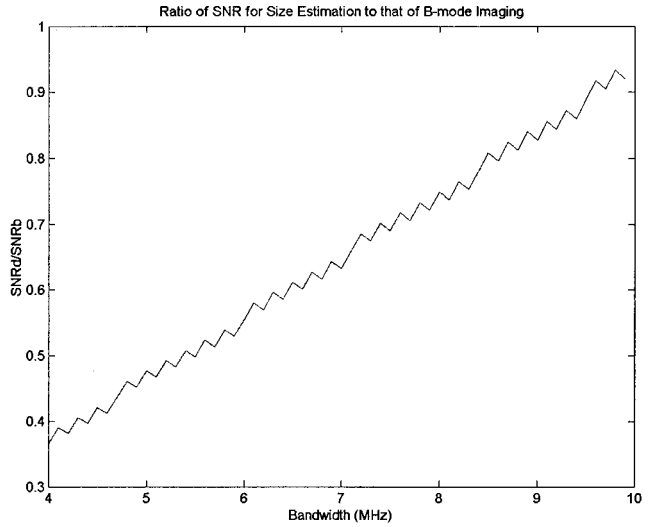

FIG. 6. Ratio of the theoretical signal to noise for size estimation to that of B-mode imaging as a function of transducer bandwidth.

$$C_z = \frac{0.9}{\mathrm{FWHM}_{\mathrm{txdcr}}}. \tag{16b}$$

Figure 5 displays the ratio of the SNRs as a function of window length for two different bandwidths. Free parameters were set to typical values, including a scatterer diameter of 100 μm, a center frequency of 5 MHz ($ka \approx 1$), and a reference waveform number effectively approaching infinity. Sample waveform number was restricted to one by the identical resolution condition. As before, the discontinuity evident in both graphs is a result of the discrete nature of the summations in Eq. (14). Although the ratio appears to be independent of window size, increasing the bandwidth from 3 to 5 MHz, improves the value. Figure 6 is a plot of the SNR ratio versus bandwidth for conditions identical to those above (fixed window length = 10 mm). Notice that the ratio increases substantially with increasing bandwidth, however, the bandwidths necessary to produce values approaching one are well above current technical limits.

VI. CONCLUSION

Expressions for the theoretical variance of backscatter coefficient and scatterer size estimates were derived. Both agreed well with experimental results. The variance of backscatter estimates was found to scale directly with the square of the backscatter coefficient being measured, and inversely with the number of power spectra used to generate estimates. The variance of size estimates decreased with increasing values of bandwidth, number of sample and reference power spectra, data segment length, and *ka*.

Although the feasibility of generating size estimates and images using a reference phantom method to estimate backscatter has been established, improvements in transducer bandwidth are necessary for performance to approach that of B-mode imaging. As a result, size imaging is most beneficial when knowledge of physical structure is necessary, or B-mode contrast is low, which occurs when scattering strength contrast and size contrast offset one another.

ACKNOWLEDGMENTS

The authors would like to extend thanks to Quan Chen, Yadong Li, Fang Dong, and Thaddeus Wilson for their technical assistance. This work was supported in part by NIH grants No. R01CA39224 and No. T32CA09206.

[1] M. Insana, Int. Rev. Exp. Pathol. **36**, 73 (1996).
[2] M. Insana and T. Hall, Ultrason. Imaging **12**, 245 (1990).
[3] M. Insana, T. Hall, J. Wood *et al.*, Invest. Radiol. **28**, 720 (1993).
[4] T. Hall, M. Insana, L. Harrison *et al.*, Ultrasound Med. Biol. **22**, 987 (1996).
[5] M. Insana and T. Hall, Phys. Med. Biol. **35**, 1373 (1990).
[6] M. Insana, R. Wagner, D. Brown *et al.*, J. Acoust. Soc. Am. **87**, 179 (1990).
[7] M. Insana, T. Hall, and L. Cook, IEEE Trans. Ultrason. Ferroelectr. Freq. Control **41**, 714 (1994).
[8] J.-F. Chen, J. Zagzebski, F. Dong *et al.*, Med. Phys. **25**, 648 (1998).
[9] P. Chaturvedi and M. Insana, J. Acoust. Soc. Am. **100**, 392 (1996).
[10] F. Lizzi, E. Feleppa, M. Astor *et al.*, IEEE Trans. Ultrason. Ferroelectr. Freq. Control **44**, 935 (1997).
[11] M. Insana and D. Brown, in *Ultrasonic Scattering in Biological Tissues*, edited by Kirk Shung (CRC Press, Boca Raton, 1993), p. 75.
[12] P. Bevington and K. Robinson, *Data Reduction and Error Analysis for the Physical Sciences*, 2nd ed. (McGraw-Hill, New York, 1992).
[13] J. Faran, J. Acoust. Soc. Am. **23**, 405 (1951).
[14] R. Wagner, M. Insana, and S. Smith, IEEE Trans. Ultrason. Ferroelectr. Freq. Control **35**, 34 (1988).
[15] When using sample and reference waveforms from the same medium, the value chosen for attenuation in the simulation code is actually irrelevant when estimating backscatter because the code does not include an additive noise term due to the measurement system.
[16] E. Feleppa, F. Lizzi, D. Coleman *et al.*, Ultrasound Med. Biol. **12**, 623 (1986).
[17] M. Oelze and W. O'Brien, Jr., J. Acoust. Soc. Am. **112**(6), 3053 (2002).
[18] L. X. Yao, J. Zagzebski, and E. Madsen, Ultrason. Imaging **12**, 58 (1990).